Progress In Electromagnetics Research C, Vol. 112, 83–98, 2021

Inset-Fed Planar Antenna Array for Dual-Band 5G MIMO Applications

Umair Rafique[1, *], Shobit Agarwal[2], Nasir Nauman[3], Hisham Khalil[3], and Khalil Ullah[4]

Abstract—An inset-fed planar MIMO antenna array has been presented for dual-band 5G applications. The proposed MIMO array offers numerous advantages such as compact size, planar structure, and high isolation. The single element of the array comprises an inset-fed rectangular patch and open circuit stubs designed on the top side of the substrate, while the bottom layer consists of a partial ground plane. Simulated and measured results show that the proposed antenna offers dual-band characteristics at 28 GHz and 38 GHz frequency bands, respectively. It has also been observed from the results that the proposed inset-fed planar antenna offers good radiation characteristics, acceptable gain, and radiation efficiency for both bands. Furthermore, a four-element-based MIMO antenna array has been designed for its possible use in 5G-enabled communication devices. It has been demonstrated that the proposed MIMO antenna provides high isolation between array elements without disturbing the characteristics of the individual antenna element. The proposed MIMO antenna array has been fabricated and measured for the validation of simulation results, and it has been observed that both the results are in good agreement.

1. INTRODUCTION

As 4th generation (4G) communication systems have gained maturity, most of the societies are now concentrating on future 5th generation (5G) communication systems [1]. One of the most demanding expectations from the upcoming 5G communication system is to provide a stable data throughput experience over a wide range. Recent studies have demonstrated the feasibility of the millimeter-wave (mm-wave) spectrum for cellular network applications [2]. With the allocation of an unlicensed spectrum, currently, at 28 GHz, 38 GHz, and 60 GHz frequency bands, it is possible to handle a high data rate with low-cost infrastructure due to increased bandwidth. However, radio propagation path loss models of lossy mm-wave channels show that a high-performance antenna system is required [3]. So, there is a need to design low-loss, compact, and low-cost antennas that can easily be integrated with mm-wave circuitry.

For mm-wave frequencies, designing an antenna is more demanding where efficiency, flexibility, and compatibility with Multi-input Multi-output (MIMO) systems are of main concern for realizing low multipath fading and high spectral efficiency [4]. With these requirements, the MIMO antenna array should provide high gain and isolation between closely placed antennas to minimize the effect of adjacent elements on the array's performance. One of the main advantages of mm-wave frequencies is that the antenna size is small, which helps to design multiple antennas in a limited space with high isolation.

In [5], a patch antenna array of 8×8 elements was reported for 28 GHz 5G applications. A pair of patch antennas were designed on both sides of the substrate, and orthogonal feed lines were used to feed

Received 13 February 2021, Accepted 15 April 2021, Scheduled 24 April 2021
* Corresponding author: Umair Rafique (rafique.1979591@studenti.uniroma1.it).
[1] Department of Information Engineering, Electronics and Telecommunications, Sapienza Università di Roma, Rome 00184, Italy. [2] Department of Electrical, Electronic and Information Technology — DEI "Guglielmo Marconi", Università di Bologna, Bologna, Italy. [3] Department of Technology, The University of Lahore, Lahore, Pakistan. [4] Department of Information Engineering and Automation, Kunming University of Science and Technology, Xishan, Kunming, China.

the patch elements. From the presented configuration, the authors achieved a gain of 20 dBi with the isolation of 20 dB between adjacent antenna elements. Although the design offered high gain, the use of orthogonal feed lines increased back and side lobe radiations. In [6], a dual-polarized wideband aperture antenna array was presented for 5G MIMO applications. The presented array consisted of 4 antenna elements, and each element had a tapered aperture hybrid structure and the backed cavity design. It was reported that the isolation between antenna elements was ≈ 18 dB, which is usually high for MIMO applications. In [7], series-fed MIMO phased arrays were presented for 28 GHz 5G applications. They were the first planar antenna arrays that offered good characteristics at mm-wave frequencies with a compact size.

An eight-element phased array was presented in [8] for dual-band 5G MIMO applications. A leaf-shaped bow-tie antenna was designed on both sides of the substrate. The designed antenna provided a wideband response in the frequency range of 25–40 GHz. It was further described that the designed MIMO antenna array performed well and offered low mutual coupling between array elements. In [9], an eight-element patch array was presented for 28/38 GHz 5G communications. The presented array consisted of eight microstrip patch antennas placed in a rectangular pattern. The presented array design performed well in the reporting bands, but the isolation between antenna elements was very poor, which restricts its use for MIMO applications.

In [10], a 16-element linear array of inset-fed microstrip patch antenna was designed for 5G applications. To enhance the bandwidth, the authors utilized a parasitic patch on top of each inset-fed patch. From the presented configuration, they demonstrated the bandwidth of 6.78 GHz starting from 24.35 to 31.13 GHz. The array elements were non-aligned to each other to achieve high isolation. However, the designed array was large, and it could not be easily integrated with portable devices. A coplanar waveguide (CPW)-fed linear antenna array was presented in [11] for 5G networks. The authors utilized a T-shaped radiator and the partial ground plane with defected ground structure (DGS) to achieve high gain, efficiency, and bandwidth. They also reported that the isolation between antenna elements was less than 22 dB, which tends to achieve high channel capacity. Furthermore, it was observed from the results that the directivity of the proposed antenna array got reduced in the broadside direction due to the use of DGS.

In [12], a tri-band 2×2 antenna array was presented for 5G applications. Two antenna elements were designed in the array, and one element was placed perpendicular to achieve better envelope correlation. Shuhrawardy et al. [13] designed a compact four-element wideband MIMO antenna for 5G services. The single antenna element consisted of a rectangular patch with an inverted-F-shaped slot, a chicken neck-shaped feed line, and a slotted ground plane. To achieve low mutual coupling, an isolation network was designed between the ground planes, which complicated the design structure. In [14], a four-element MIMO antenna design was presented. The antenna elements were placed on each side of the substrate. Each element consisted of an array of a pair of elements. For improved radiation characteristics, DGS was used, and for enhanced isolation, the polarization diversity technique was employed between the radiators. From the above-presented designs, it has been observed that they were either large, consisted of complex structures, or did not offer better performance for 5G applications.

In this paper, an inset-fed planar antenna design with a four-element MIMO configuration is presented for 5G networks. It is described that the designed antenna offers dual-band characteristics in the mm-wave spectrum, and it has high gain and efficiency for the bands of interest. Furthermore, the designed MIMO antenna array has a compact size and provides good isolation between antenna elements. It is also described that the designed MIMO antenna offers almost equal or better characteristics than the designs presented in [5–14].

2. SINGLE ELEMENT DESIGN

2.1. Antenna Geometry

The proposed dual-band inset-fed planar antenna design is depicted in Figs. 1(a), (b), and the prototype of the fabricated antenna is shown in Figs. 2(a), (b). The overall design parameters of the proposed antenna are listed in Table 1. A 50 Ω microstrip feed line based inset-fed rectangular patch is designed on the top side of a Rogers RT/Duroid 5880 substrate having $\varepsilon_r = 2.2$, $h = 0.787$ mm, and $\tan\delta = 0.0009$

(@10 GHz) with two open-circuit stubs, and a partial ground plane is designed on the bottom layer. The overall dimensions of the proposed dual-band antenna are $10 \times 10\,\text{mm}^2$.

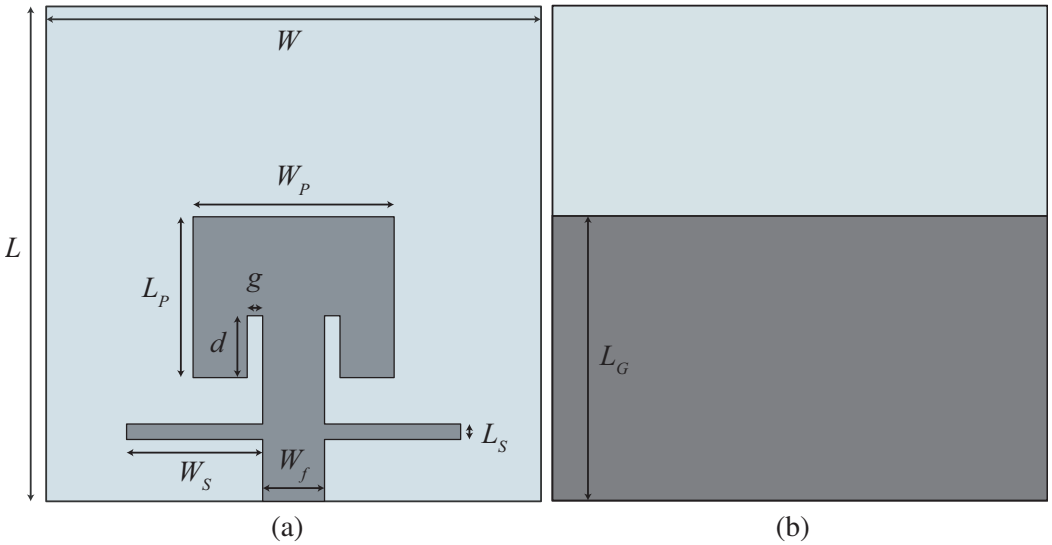

Figure 1. Design of the proposed inset-fed planar antenna. (a) Front view. (b) Back view.

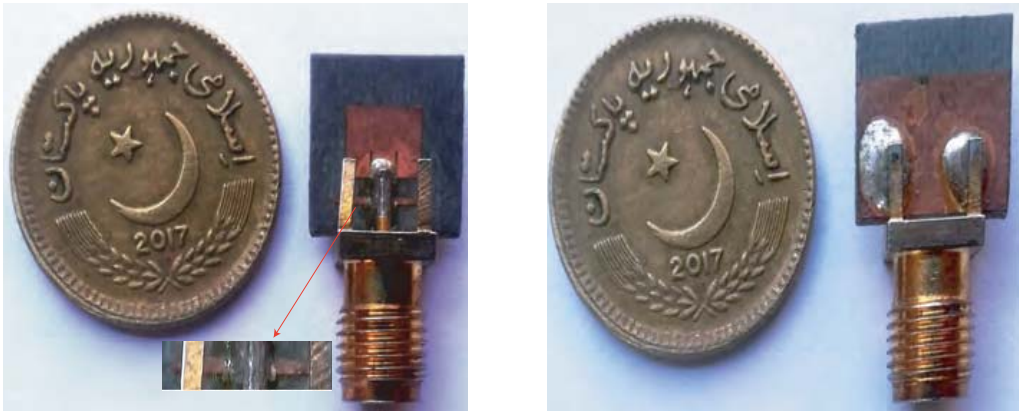

Figure 2. Fabricated prototype of the proposed inset-fed planar antenna. (a) Front view. (b) Back view.

Table 1. Design parameters of the proposed inset-fed planar antenna.

Parameters	Value (mm)	Parameters	Value (mm)
L	10	W	10
L_P	4	W_P	5
d	1.5	g	0.2
L_S	0.3	W_S	2.5
W_f	1.5	L_G	7

2.2. Design Principle

Initially, an inset-fed planar antenna has been designed with a partial ground plane, shown in the inset of Fig. 3, to check its response for the proposed application, and its reflection coefficient, S_{11}, is shown in Fig. 3. From the figure, it has been observed that the inset-fed planar antenna resonates at 38 GHz frequency band. After that, two open-circuit stubs are placed with the feed line, and it has been observed that when the length of stubs is taken nearly quarter wavelength (at 28 GHz), it offers inductive or capacitive impedance around the resonant frequency of the patch antenna and realizes dual-band response [15]. So, it is clear from the result of Fig. 3 that the addition of open-circuit stubs with the feed line provides resonance at 28 GHz frequency band.

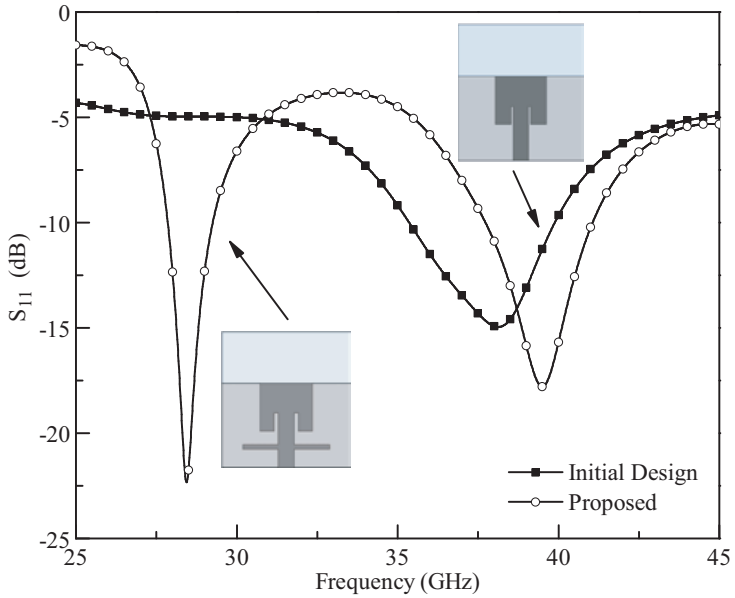

Figure 3. Simulated S_{11} of different antenna designs (inset of figure shows initial and proposed antenna designs).

To validate the proposed methodology, the surface current distribution of the proposed dual-band inset-fed planar antenna is plotted as shown in Fig. 4. It is observed from Fig. 4 that for both resonant frequencies, a dense current is distributed on open circuit stubs and at the inset point. So, it is worth

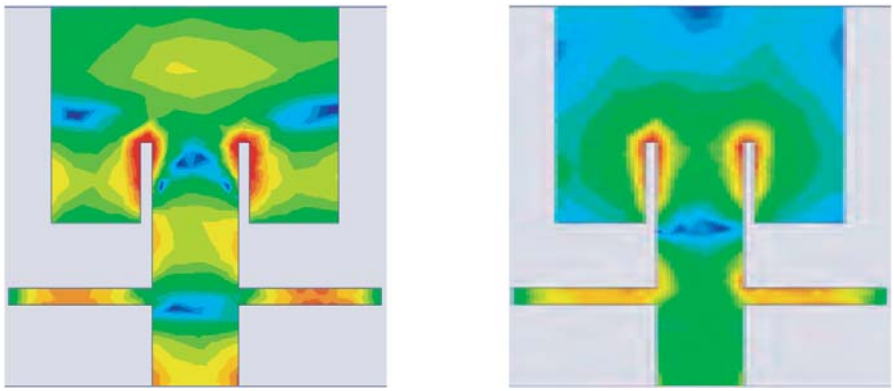

Figure 4. Surface current distribution of the proposed inset-fed planar antenna for (a) 28.44 GHz and (b) 39.49 GHz.

mentioning here that the inset-fed technique with open-circuit stubs plays an important role in achieving dual-band characteristics.

2.3. Equivalent Circuit Model

Figure 5 shows the equivalent circuit of the proposed inset-fed planar antenna. One can model the inset-fed patch by using the transmission line model because it is simple to implement [16]. The problem with the transmission line model is that it does not take into account different structure behaviors that exist in the configuration of an inset-fed patch antenna. So, in this paper, an equivalent circuit model is designed by utilizing the technique presented in [17] as shown in Fig. 5. The radiating stubs can be modeled by using a combination of series and parallel RLCs [18] as shown in Fig. 5.

A comparison between EM and circuit model simulations is shown in Fig. 6. From the figure, one can observe that S_{11} of the proposed equivalent circuit model is in good agreement with the simulated

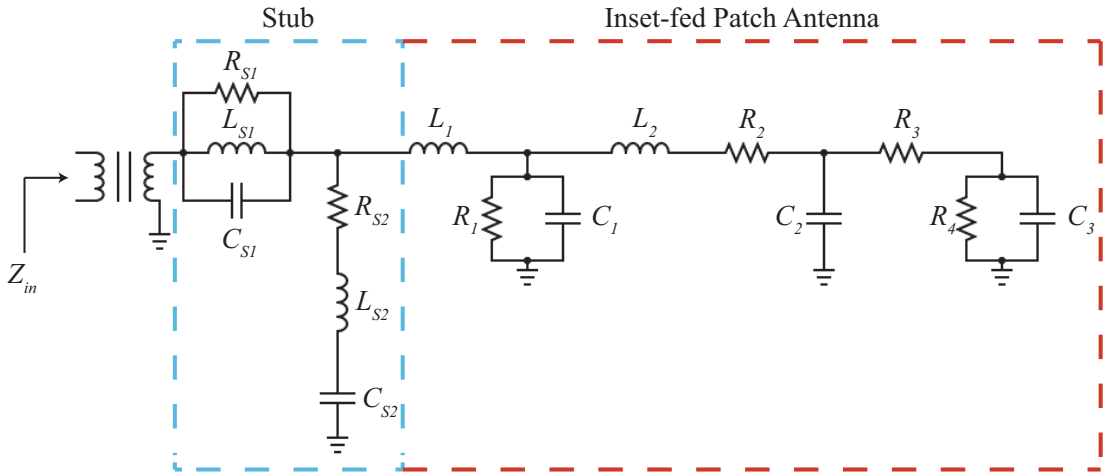

Figure 5. Equivalent circuit model of the proposed inset-fed planar antenna.

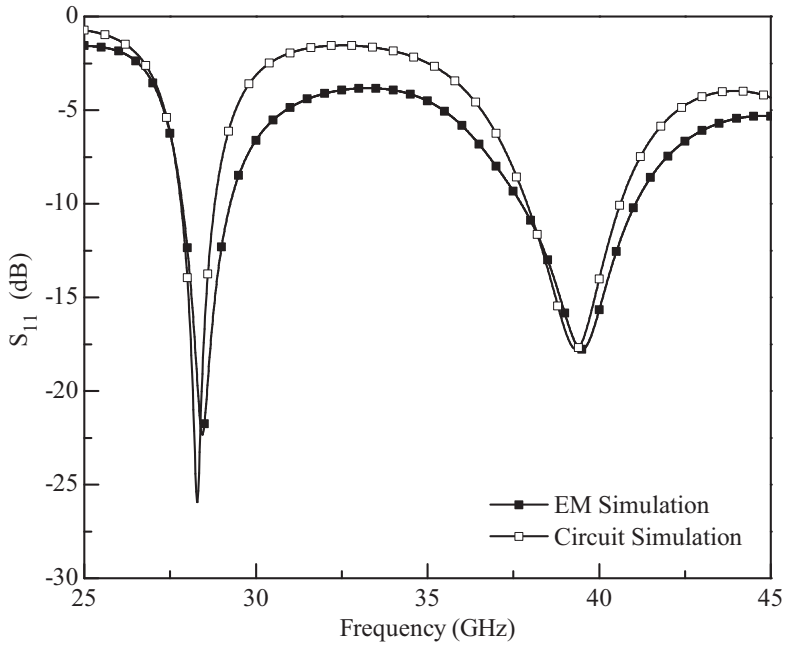

Figure 6. EM simulated and equivalent circuit S_{11} of the proposed inset-fed planar antenna.

data. The optimized equivalent circuit parameters are: $R_{s1} = 5\,\text{k}\Omega$, $L_{s1} = 0.27\,\text{nH}$, $C_{s1} = 0.26\,\text{pF}$, $R_{s2} = 40\,\Omega$, $L_{s2} = L_1 = 0.4\,\text{nH}$, $C_{s2} = C_1 = C_2 = 0.01\,\text{pF}$, $R_1 = 40\,\Omega$, $L_2 = 0.1\,\text{nH}$, $R_2 = 2\,\text{k}\Omega$, $R_3 = R_4 = 25\,\Omega$, $C_3 = 0.1\,\text{pF}$.

2.4. Parametric Analysis

A parametric analysis of design parameters g, d, and W_S is conducted to observe their effects on the antenna's performance, and the results are shown in Fig. 7. It is observed from Fig. 7(a) that when the value of g is increased from 0.2 mm to 1 mm, both the resonant frequencies shift towards the lower bands, which means that the change in g will increase the electrical dimensions of the antenna.

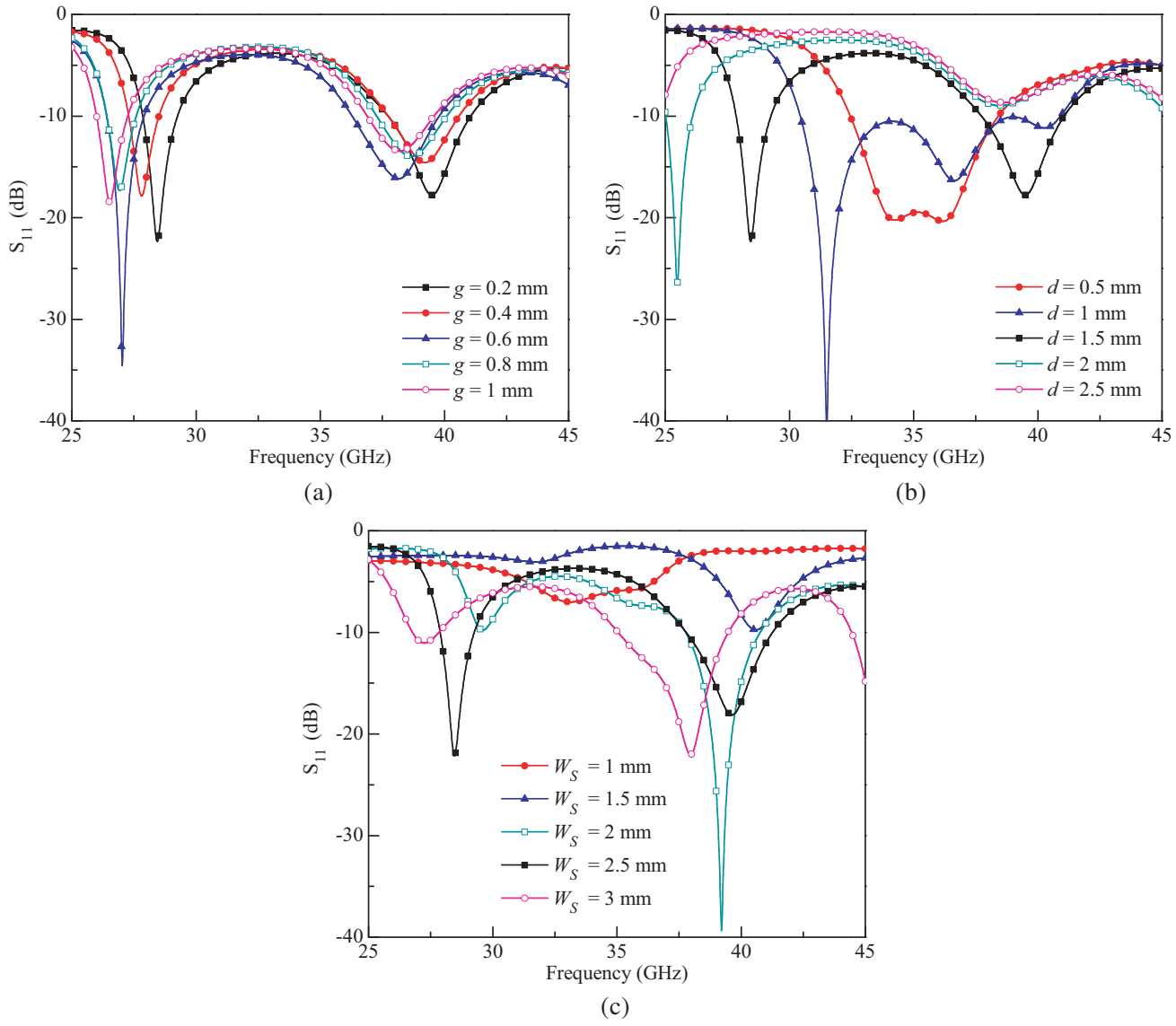

Figure 7. Antenna's performance with variations in (a) g, (b) d, and (c) W_S.

It is a known fact that for inset-fed patch antenna design, the antenna's impedance mainly depends upon inset length. This effect can be seen from the result of Fig. 7(b) where a parametric study has been conducted by changing the inset length d. When the value of d is changed in the range of 0.5–2.5 mm, a change in the antenna's impedance is observed. For $d = 0.5\,\text{mm}$ and 1 mm, the antenna provides

a wideband response in the frequency range of 32.45–38.41 GHz and 30.44–40.91 GHz, respectively, as shown in Fig. 7(b). For values > 1.5 mm, only one resonance is observed around 25 GHz, which means that the antenna's impedance matches well for 25 GHz frequency band.

The stub length also plays an important role to get desired resonant frequencies; therefore, a parametric study has also been conducted to observe the effect of W_S on antenna's performance. From Fig. 6, it is observed that the equivalent circuit model of stubs is more like a band-stop filter design, which means that the stubs will behave as a band-stop filter. From Fig. 7(c), it can be observed that for $W_S < 2$ mm, no resonance occurs in the band of interest, while for $W_S > 2.5$ mm, a minor shift in the resonant frequencies is observed.

2.5. Results and Discussion

The results of the dual-band inset-fed planar antenna are described in the following subsections. Particular features such as reflection coefficient, gain, efficiency, and radiation characteristics are described to evaluate its performance.

2.5.1. Reflection Coefficient

Figure 8 illustrates S_{11} of the proposed inset-fed planar antenna. It is observed from Fig. 8 that the proposed antenna offers dual-band characteristics. The noted resonant frequencies are 28.44 GHz and 39.49 GHz, and according to the -10 dB bandwidth criterion, the impedance bandwidths of the two bands are 1.39 GHz and 3.33 GHz. To validate simulation results, the prototype, shown in Fig. 2, is measured using Agilent Technologies Power Network Analyzer (PNA) N5245B, and the respective results are given in Fig. 8. Measured results show that the proposed antenna resonates well in the bands of interest. Some discrepancies are observed in the measured results, which are due to fabrication tolerances and SMA connector losses.

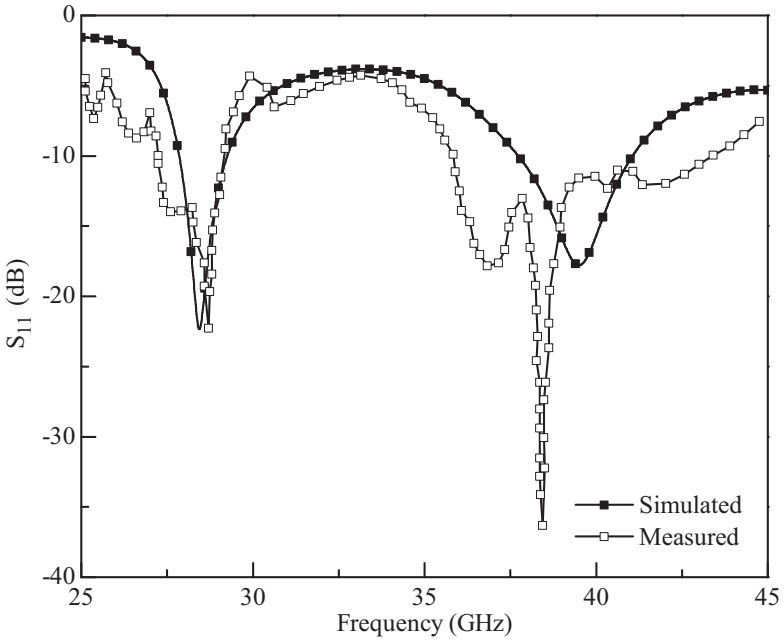

Figure 8. Simulated and measured S_{11} of the proposed inset-fed planar antenna.

2.5.2. Realized Gain and Efficiency

The results of the realized gain of the proposed antenna are depicted in Fig. 9(a). For desired resonant frequencies (28.44 GHz and 39.49 GHz), the simulated gain values are noted to be 5.59 dBi and 5.70 dBi,

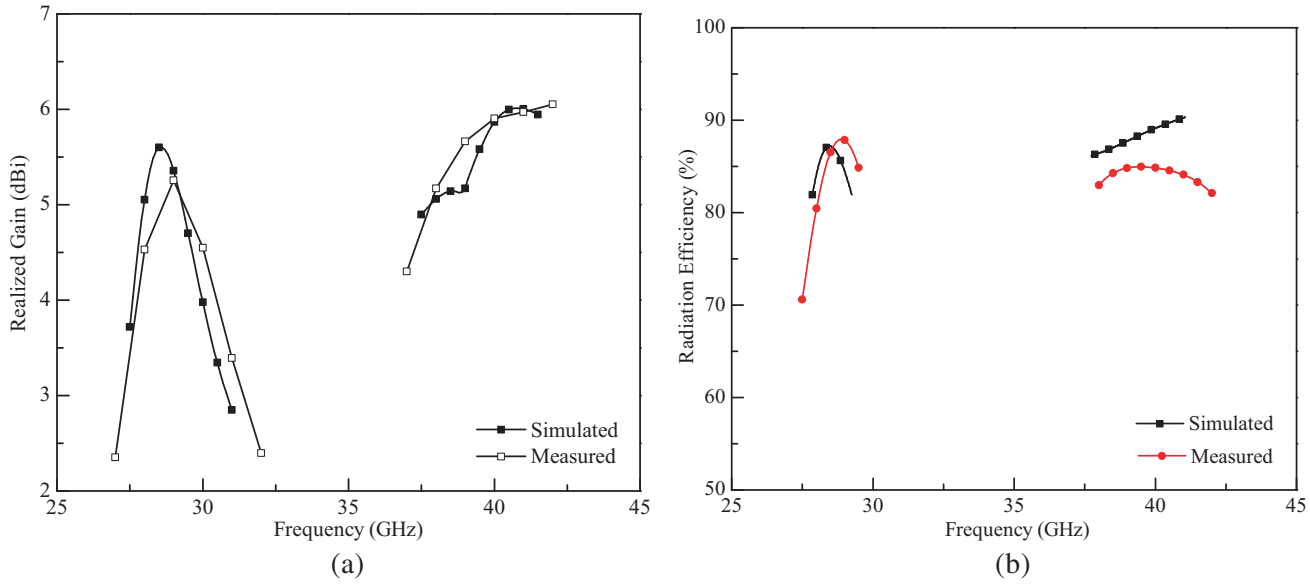

Figure 9. Simulated and measured (a) realized gain and (b) radiation efficiency of the proposed inset-fed planar antenna.

while the measured gain values are noted to be 5.25 dBi and 5.90 dBi. Fig. 9(b) illustrates simulated and measured radiation efficiencies of the proposed antenna. From the figure, it has been observed that an average efficiency (simulated) of 88% is observed for both the bands. On the other hand, the average measured radiation efficiency for both bands is 84%.

2.5.3. Radiation Characteristics

The radiation characteristics of the proposed inset-fed planar antenna for E-plane ($\phi = 0°$) and H-plane ($\phi = 90°$) at 28.44 GHz and 39.49 GHz are depicted in Fig. 10. For 28.44 GHz, shown in Fig. 10(a), butterfly-like radiation characteristics are observed for E-plane, while for H-plane, shown in Fig. 10(b), broadside radiation characteristics are observed. It can also be observed from the result of Fig. 10(b) that the main beam is titled towards 50°. For 39.49 GHz, shown in Figs. 10(c), (d), almost omnidirectional radiation characteristics are observed for both E- and H-planes. The discrepancies between the results are observed that can arise due to fabrication tolerances and scattering measurement environment.

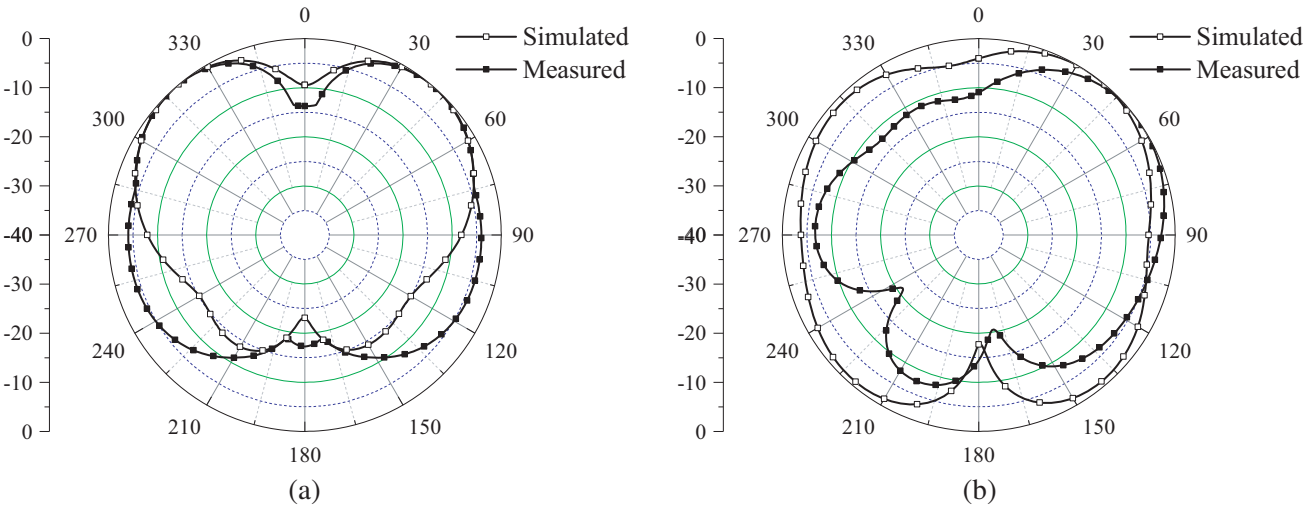

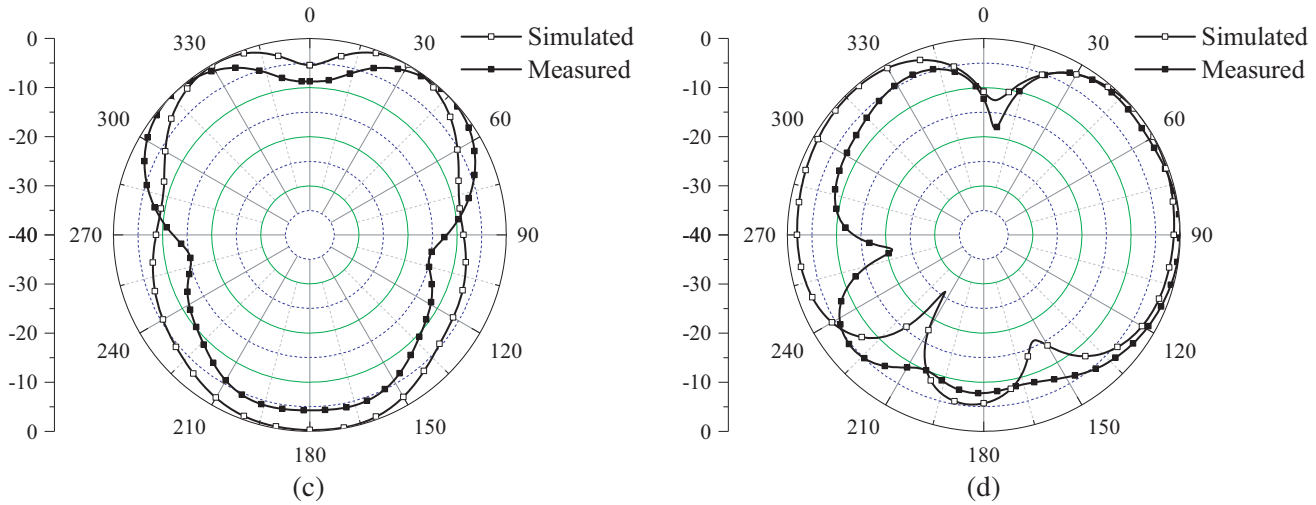

Figure 10. Simulated and measured radiation characteristics of the proposed inset-fed planar antenna. (a) E-plane (28.44 GHz). (b) H-plane (28.44 GHz). (c) E-plane (39.49 GHz). (d) H-plane (39.49 GHz).

3. PROPOSED MIMO ANTENNA ARRAY

3.1. Array Geometry

The next step is to design a four-element-based MIMO antenna array for 5G-enabled communication devices. The four antenna elements are designed on a single substrate by keeping in mind the conventional array design methodology. According to the theory of conventional array design, the minimum distance between antenna elements should be equal to or greater than $\lambda/2$ to reduce coupling effects. Therefore, a gap about 0.5 mm is created between antenna elements, and each element's width is increased from 10 to 10.5 mm, which is also related to the gap between two antenna elements denoted as S. This design technique does not allow antenna elements to correlate and also improves isolation. For array design, the width of the substrate, denoted as W_a, is increased, while other design dimensions remain the same. Figs. 11(a), (b) show the design and configuration of the proposed MIMO antenna array. The proposed MIMO antenna array is also fabricated, and the prototype is shown in Figs. 12(a), (b).

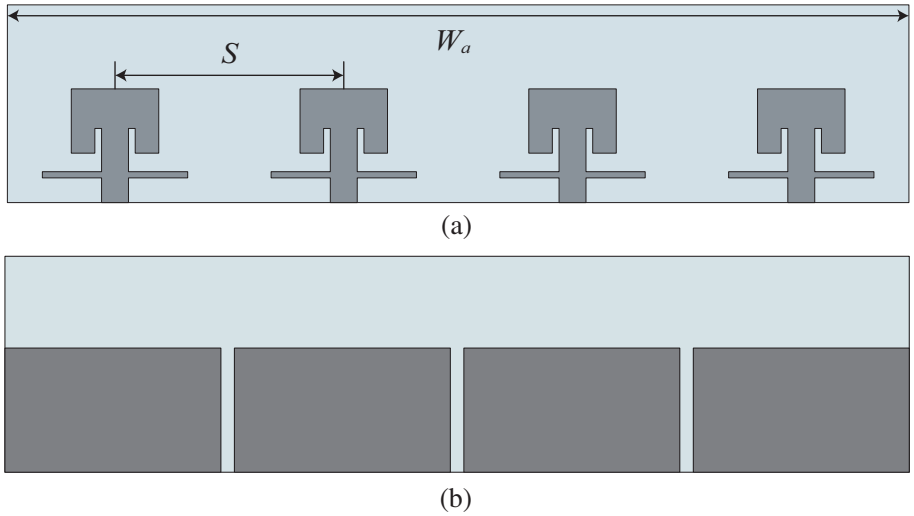

Figure 11. Proposed four-element MIMO antenna array for 5G applications. (a) Front view. (b) Back view.

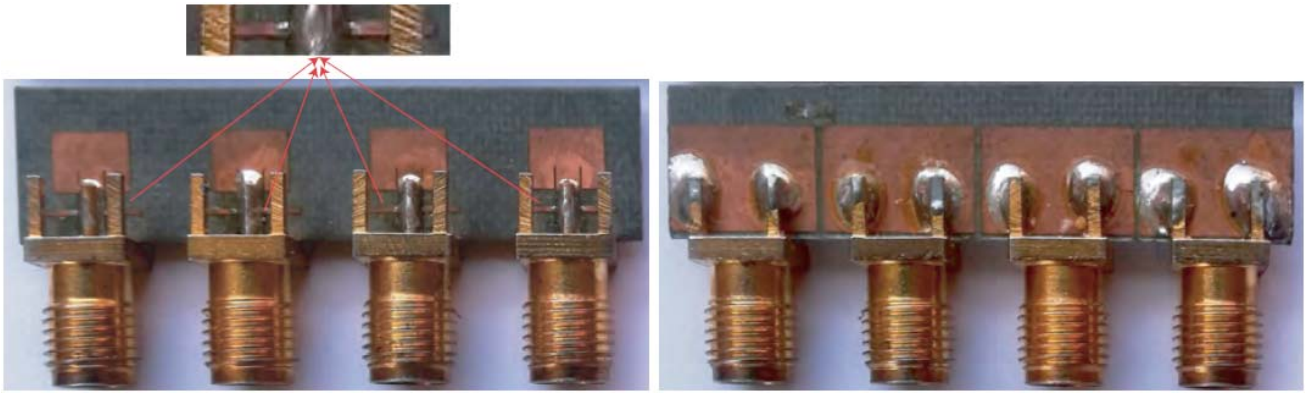

(a) (b)

Figure 12. Fabricated prototype of the proposed four-element MIMO antenna array. (a) Front view. (b) Back view.

3.2. Results and Discussion

In the following subsections, the performance of the proposed MIMO antenna array is described. The performance is investigated in terms of reflection coefficient, isolation between antenna elements, radiation characteristics, envelop correlation coefficient, diversity gain, and mean effective gain.

3.2.1. Reflection Coefficient

Figure 13 depicts the simulated and measured reflection coefficients of the proposed MIMO antenna array. For better visualization, the simulated and measured curves of S_{11} and S_{22} are presented. From the figure, it is observed that the proposed MIMO antenna array provides an acceptable reflection coefficient for the bands of interest. Some discrepancies between simulated and measured results are noted, which could be associated with fabrication tolerances, imperfect soldering of SMA connectors, and their losses.

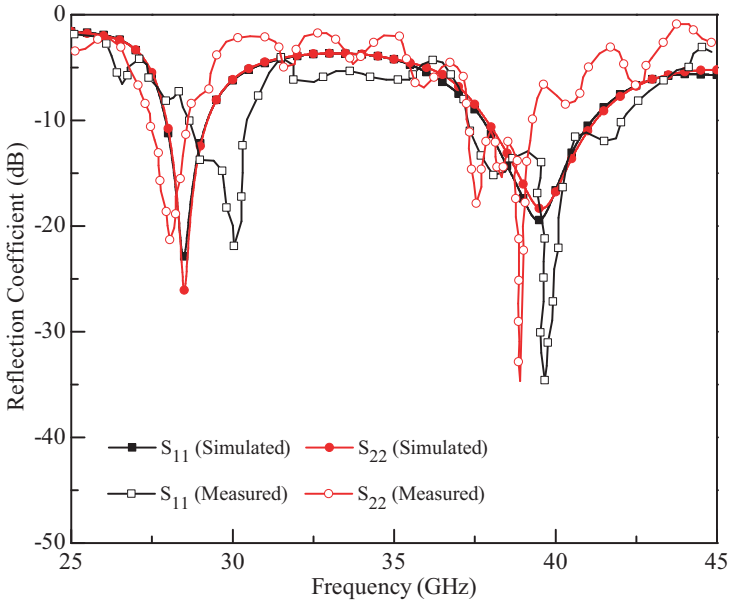

Figure 13. Simulated and measured reflection coefficient of the proposed MIMO antenna array.

3.2.2. Transmission Coefficient

The simulated and measured transmission coefficient results of the proposed MIMO antenna array are shown in Fig. 14. A good agreement is observed between the simulated and measured transmission coefficients. One can also observe from the results of Fig. 14 that the isolation between two adjacent antenna elements is less than 25 dB, which ensures low mutual coupling between array elements. The reason behind reduced isolation is that each array element has an independent ground plane, which does not allow the current to move from one element to another. This effect can also be observed in Fig. 15, where the surface current distribution of the proposed MIMO antenna array is presented. The plot of Fig. 15 is extracted by exciting only antenna 1 of the MIMO array. These results also validate the high performance of the proposed dual-band MIMO antenna array.

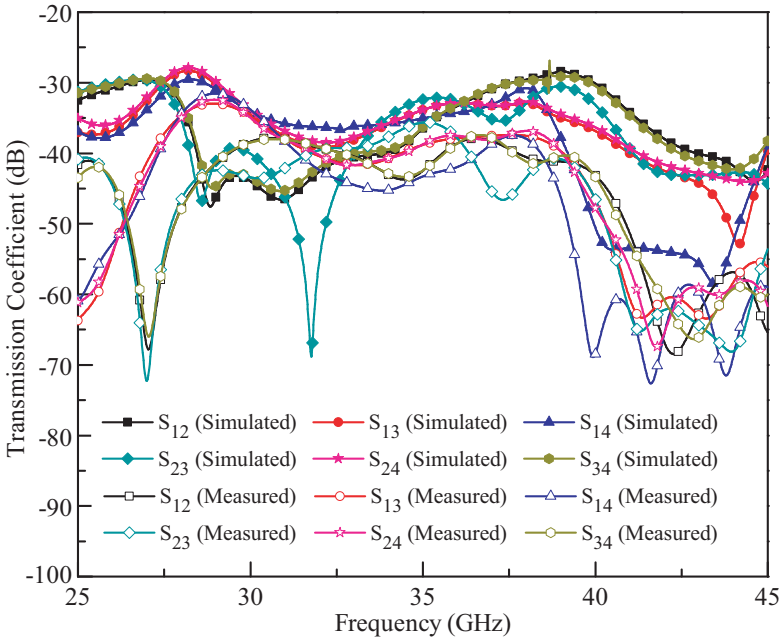

Figure 14. Simulated and measured transmission coefficient results of the proposed MIMO antenna array.

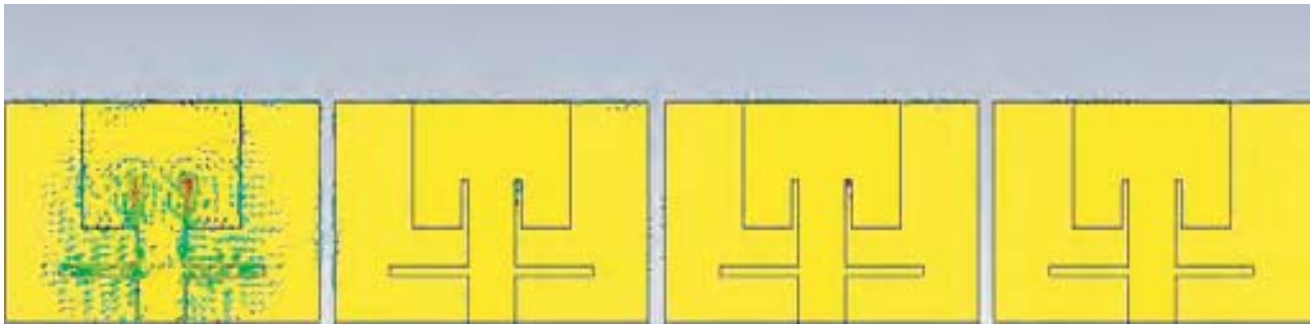

Figure 15. Surface current distribution of the proposed MIMO antenna array.

3.2.3. Radiation Characteristics

The simulated and measured radiation characteristics of the proposed MIMO antenna array for E-($\phi = 0°$) and H-planes ($\phi = 90°$) for resonant frequencies 28.44 GHz and 39.49 GHz are depicted in

Figs. 16(a)–(d). The antenna is tested in an anechoic chamber using a standard procedure. A horn antenna is used as a reference antenna, and the proposed MIMO antenna array is placed on the other side. To measure the radiation pattern in both the planes, two different measurements are carried out where the proposed array is placed horizontally and vertically for $\phi = 0°$ and $90°$, respectively. For 28.44 GHz, in the case of E-plane, omnidirectional radiation characteristics are observed (shown in Fig. 16(a), while for H-plane, directional radiation characteristics are observed as shown in Fig. 16(b). For 39.49 GHz (Fig. 16(c) and 16(d)), the antenna demonstrates an approximately directional radiation pattern in E-plane and nearly omnidirectional pattern in H-plane. The cross-polarization component is less at some angles. However, for some angles, the level of cross-polarization is high, shown in Figs. 16(a)–(d), which is due to the excitation of hybrid modes at higher frequencies [19]. Moreover, the thickness of the substrate is less than the quarter wavelength therefore, and a 180° phase difference is introduced between the reflected surface waves and the waves that impinge on the substrate. Due to this phenomenon, destructive interference will be produced, which results in the increment of the cross-polarized field [19, 20].

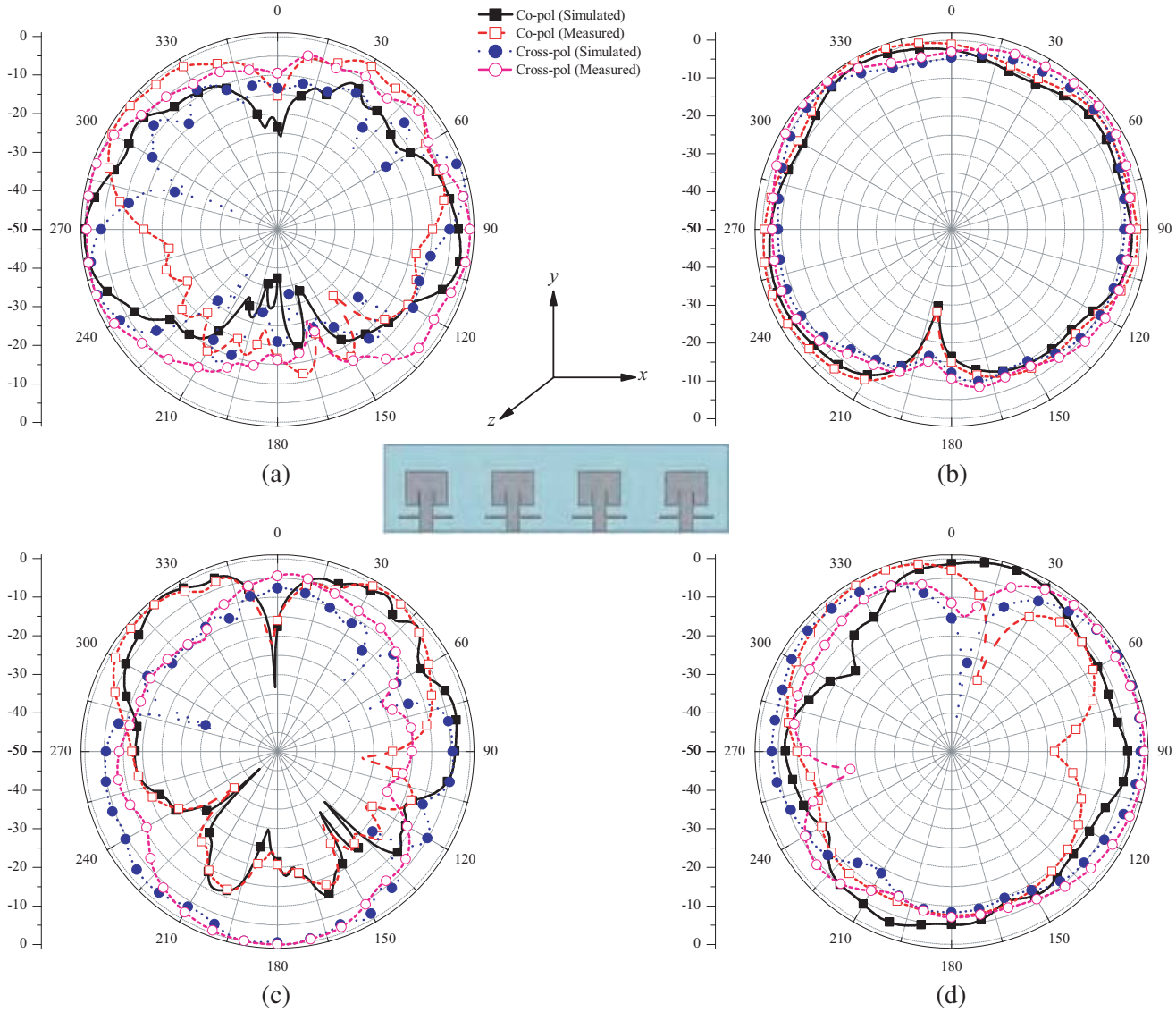

Figure 16. Simulated and measured radiation characteristics of the proposed MIMO antenna array. (a) E-plane (28.44 GHz). (b) H-plane (28.44 GHz). (c) E-plane (39.49 GHz). (d) H-plane (39.49 GHz).

3.2.4. Envelope Correlation and Diversity Gain

The envelope correlation coefficient (ECC) is an important factor to evaluate the MIMO system's performance. It measures the degree of similarity among the received signals. In an ideal scenario, the MIMO system requires an ECC equal to zero. The correlation between the radiation patterns of MIMO elements can also be evaluated using ECC. So, ECC can be calculated by using the radiation characteristics of the MIMO antenna as [21]

$$ECC = \frac{\int_{4\pi} E_i(\theta,\phi).E_j^*(\theta,\phi)d\Omega}{\sqrt{\int_{4\pi} E_i(\theta,\phi).E_i^*(\theta,\phi)d\Omega \int_{4\pi} E_j(\theta,\phi).E_j^*(\theta,\phi)d\Omega}} \tag{1}$$

where E_i and E_j represent far-field radiation characteristics for ports i and j.

For the proposed array configuration, the value of ECC is approximately equal to zero for the desired frequency bands as shown in Fig. 17. This result also demonstrates good isolation between antenna elements, which is an important factor for simultaneous operation.

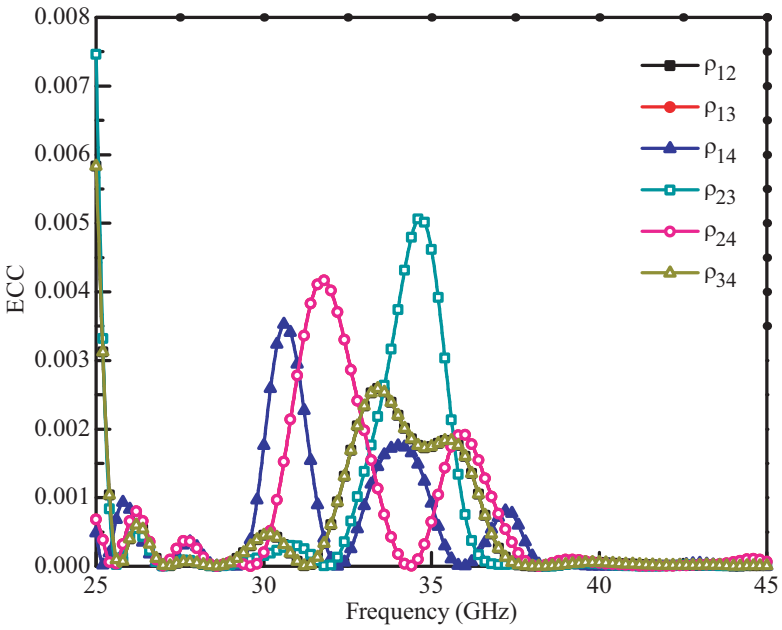

Figure 17. Envelope correlation coefficient results of the proposed MIMO antenna array.

Diversity gain (DG) is another important parameter to assess the performance of MIMO antennas. It can be calculated as [22]:

$$DG\,(\text{dB}) = 10\log\left(\sqrt{1 - ECC^2}\right) \tag{2}$$

Figure 18 shows the diversity gain of the proposed MIMO antenna array. It is observed from the figure that the proposed MIMO antenna has DG > 9.96 dB for both bands.

3.2.5. Mean Effective Gain

In a fading environment, mean effective gain (MEG) is the measure of the amount of power received by the antenna elements compared to an isotropic antenna. One can compute the MEG as [22]:

$$MEG_i = 0.5\left[1 - \sum_{j=1}^{N} |S_{ij}|^2\right] \leq -3\,\text{dB} \tag{3}$$

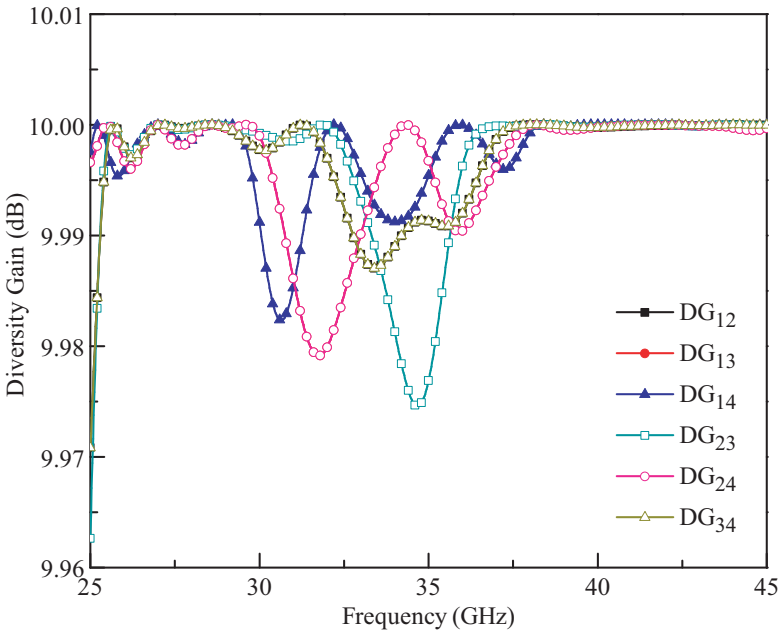

Figure 18. Diversity gain results of the proposed MIMO antenna array.

The MEG_1 and MEG_2 can be written as [22]:

$$MEG_1 = 0.5\left[1 - |S_{11}|^2 - |S_{12}|^2 - |S_{13}|^2 - |S_{14}|^2\right] \quad (4)$$

$$MEG_2 = 0.5\left[1 - |S_{21}|^2 - |S_{22}|^2 - |S_{23}|^2 - |S_{24}|^2\right] \quad (5)$$

Also,

$$MEG_1 - MEG_2 \leq 3\,\text{dB} \quad (6)$$

MEG_3 and MEG_4 can also be evaluated using Equation (3). For our proposed MIMO configuration, the value of MEG_1 and MEG_2 is less than -3 dB, which is also clear from the result of Fig. 19. It can

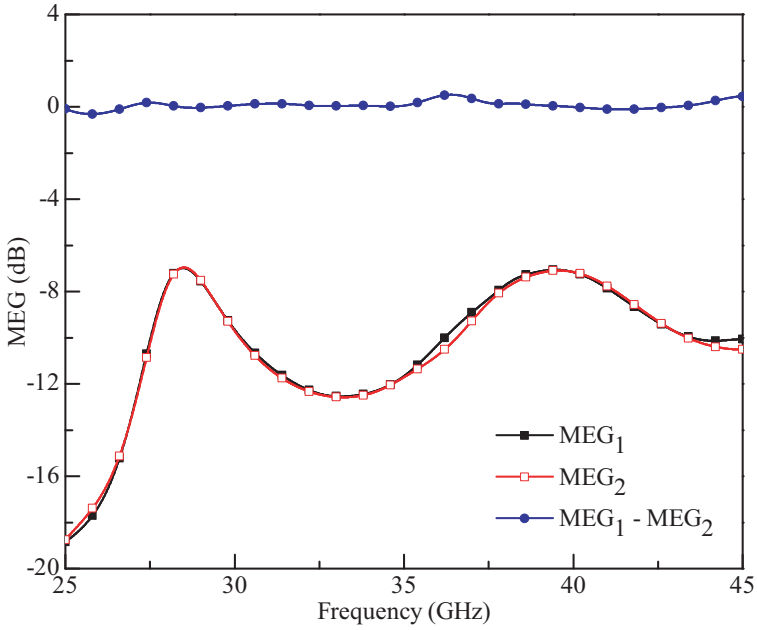

Figure 19. Mean effective gain of the proposed MIMO antenna array.

Table 2. Comparison between previously presented and proposed 5G MIMO antenna arrays.

Ref.	Array Size (mm^3)	Substrate	ε_r	Frequency (GHz)	Isolation (dB)	Gain (dBi)	Efficiency (%)
[5]	–	Duroid 5880	2.2	28	20	3.6	–
[6]	25×25×1.8	Duriod 5880	2.2	26–34.6	18	6.7	80
[7]	–	Duroid 5880	2.2	27.3–29	29	7.73	88
[8]	$36.8 \times 4.6 \times 0.5$	AR 350	3.5	25–40	10	5	90
[9]	$16 \times 15 \times 1.6$	FR-4	4.4	28/38	10	5.5	–
[10]	$99.2 \times 17.45 \times 0.25$	Duroid 5880	2.2	24.3–31.2	20	8.2	–
[11]	$50.8 \times 12 \times 0.8$	Duroid 5880	2.2	25–37.5	22	–	–
[12]	$40 \times 20 \times 0.787$	Duroid 5880	2.2	28/38/60	–	–	–
[13]	$25 \times 30 \times 0.8$	Duroid 5880	2.2	26.6–40.3	20	5.57	–
[14]	$30 \times 35 \times 0.76$	RO4350B	3.66	25.5–29.6	17	8	–
Proposed	$41.5 \times 8 \times 0.787$	Duroid 5880	2.2	28/38	25	5.5	84

be observed from the figure that the difference between MEG_1 and MEG_2 is less than 3 dB.

A comparison between the proposed and previously reported MIMO antenna arrays is presented in Table 2. The comparison is done in terms of array size, substrate used, dielectric constant of the substrate, isolation between antenna elements, gain, and radiation efficiency of the single antenna element. It is observed from the data of Table 2 that the proposed MIMO antenna array offers good characteristics with compact size.

4. CONCLUSION

An inset-fed dual-band planar antenna design has been presented for 5G applications along with MIMO configuration. The proposed antenna design consists of an inset-fed rectangular patch element, open circuit stubs, and a partial ground plane. It is shown that the inset-fed configuration with open-circuit stubs provides dual-band characteristics. It is also shown that the proposed antenna offers average realized gain and radiation efficiency of 5.5 dBi and 84% for both the bands, respectively. Furthermore, a four-element antenna array is designed to demonstrate the performance of the proposed antenna for 5G MIMO applications. The results of the MIMO configuration demonstrate low mutual coupling and good isolation characteristics between adjacent antenna elements. From the presented results, it is noted that the proposed antenna is suitable for 5G MIMO applications.

REFERENCES

1. Rappaport, T. S., et al., "Millimeter wave mobile communications for 5G cellular: It will work!," *IEEE Access*, Vol. 1, No. 1, 335–349, 2013.
2. Rappaport, T. S., et al., "Cellular broadband millimeter wave propagation and angle of arrival for adaptive beam steering systems (Invited Paper)," *IEEE Radio and Wireless Symposium (RWS)*, 151–154, 2012.
3. Sulyman, A. I., et al., "Radio propagation path loss models for 5G cellular networks in the 28 GHz and 38 GHz millimeter-wave bands," *IEEE Communications Magazine*, Vol. 52, No. 9, 78–86, 2014.
4. Wu, D., S. W. Cheung, T. I. Yuk, and X. L. Sun, "A planar MIMO antenna for mobile phones," *PIERS Proceedings*, 1150–1152, Taipei, March 25–28, 2013.
5. Haraz, O. M., M. M. Ashraf, and S. Alshebili, "8×8 patch antenna array with polarization and space diversity for future 5G cellular applications," *International Conference on Information and Communication Technology Research*, 258–261, 2015.

6. Liu, S. T., Y. W. Hsu, and Y. C. Lin, "A dual polarized cavity-backed aperture antenna for 5G mmW MIMO applications," *IEEE International Conference on Microwaves, Communications, Antennas and Electronic Systems (COMCAS)*, 1–5, 2015.
7. Khalily, M., R. Tafazolli, T. Rahman, and M. Kamarudin, "Design of phased arrays of series-fed patch antennas with reduced number of the controllers for 28 GHz mm-wave applications," *IEEE Antennas and Wireless Propagation Letters*, Vol. 15, 1305–1308, 2016.
8. Parchin, N. O., M. Shen, and G. F. Pedersen, "End-fire phased array 5G antenna design using leaf-shaped bow-tie elements for 28/38 GHz MIMO applications," *2016 IEEE International Conference on Ubiquitous Wireless Broadband (ICUWB)*, 1–4, 2016.
9. Rafique, U., H. Khalil, and S. Rehman, "Dual-band microstrip patch antenna array for 5G mobile communications," *2017 Progress In Electromagnetics Research Symposium — Fall (PIERS — FALL)*, Singapore, November 19–22, 2017.
10. Khalily, M., R. Tafazolli, P. Xiao, and A. A. Kishk, "Broadband mm-Wave microstrip array antenna with improved radiation characteristics for different 5G applications," *IEEE Transactions on Antennas and Propagation*, Vol. 66, No. 9, 4641–4647, 2018.
11. Jilani, S. F. and A. Alomainy, "Millimetre-wave T-shaped MIMO antenna with defected ground structures for 5G cellular networks," *IET Microwave, Antennas & Propagation*, Vol. 12, No. 5, 672–677, 2018.
12. Chu, S., M. N. Hasan, J. Yan, and C. C. Chu, "Tri-band 2×2 5G MIMO antenna array," *Asia-Pacific Microwave Conference (APMC)*, 1543–1545, 2018.
13. Shuhrawardy, M., M. H. M. Chowdhury, and R. Azim, "A four-element compact wideband MIMO antenna for 5G applications," *International Conference on Electrical, Computer and Communication Engineering (ECCE)*, 1–5, 2019.
14. Khalid, M., et al., "4-port MIMO antenna with defected ground structure for 5G millimeter wave applications," *Electronics*, Vol. 9, No. 71, 1–13, 2020.
15. Du Plessis, M. and J. Cloete, "Tuning stubs for microstrip-patch antennas," *IEEE Antennas and Propagation Magazine*, Vol. 36, No. 6, 52–56, 1994.
16. Balanis, C. A. *Antenna Theory: Analysis and Design*, John Wiley & Sons, 2016.
17. Chouchene, W., C. Larbi, and T. Aguili, "New electrical equivalent circuit model of the inset fed rectangular patch antenna," *2017 Progress In Electromagnetics Research Symposium — Fall (PIERS — FALL)*, Singapore, November 19–22, 2017.
18. Iqbal, A., et al., "A compact UWB antenna with independently controllable notch bands," *Sensors*, Vol. 19, No. 6, 1–12, 2019.
19. Rahman, S., Q. Cao, H. Ullah, and H. Khalil, "Compact design of trapezoid shape monopole antenna for SWB application," *Microwave and Optical Technology Letters*, Vol. 61, 1931–1937, 2019.
20. Ludwig, A. C., "The definition of cross polarization," *IEEE Transactions on Antennas and Propagation*, Vol. 21, No. 1, 116–119, 1973.
21. Cornelius, R., A. Narbudowicz, M. J. Ammann, and D. Heberling, "Calculating the envelope correlation coefficient directly from spherical modes spectrum," *2017 11th European Conference on Antennas and Propagation*, 2017.
22. Kumar, A., A. Q. Ansari, B. K. Kanaujia, and J. Kishor, "High isolation compact four-port MIMO antenna loaded with CSRR for multiband applications," *Frequenz*, Vol. 72, No. 9–10, 415–427, 2018.